nature COMMUNICATIONS

ARTICLE

https://doi.org/10.1038/s41467-021-27041-w OPEN

Evidence for anisotropic spin-triplet Andreev reflection at the 2D van der Waals ferromagnet/superconductor interface

Ranran Cai[1,2,7], Yunyan Yao[1,2,7], Peng Lv[3], Yang Ma[1,2], Wenyu Xing[1,2], Boning Li[1,2], Yuan Ji[1,2], Huibin Zhou[1,2], Chenghao Shen[4], Shuang Jia[1,2,5,6], X. C. Xie[1,2,5,6], Igor Žutić[4], Qing-Feng Sun[1,2,5,6] & Wei Han[1,2✉]

Fundamental symmetry breaking and relativistic spin–orbit coupling give rise to fascinating phenomena in quantum materials. Of particular interest are the interfaces between ferromagnets and common s-wave superconductors, where the emergent spin-orbit fields support elusive spin-triplet superconductivity, crucial for superconducting spintronics and topologically-protected Majorana bound states. Here, we report the observation of large magnetoresistances at the interface between a quasi-two-dimensional van der Waals ferromagnet $Fe_{0.29}TaS_2$ and a conventional *s*-wave superconductor NbN, which provides the possible experimental evidence for the spin-triplet Andreev reflection and induced spin-triplet superconductivity at ferromagnet/superconductor interface arising from Rashba spin-orbit coupling. The temperature, voltage, and interfacial barrier dependences of the magnetoresistance further support the induced spin-triplet superconductivity and spin-triplet Andreev reflection. This discovery, together with the impressive advances in two-dimensional van der Waals ferromagnets, opens an important opportunity to design and probe superconducting interfaces with exotic properties.

[1] International Center for Quantum Materials, School of Physics, Peking University, 100871 Beijing, P. R. China. [2] Collaborative Innovation Center of Quantum Matter, 100871 Beijing, P. R. China. [3] Department of Physics, Wuhan University of Technology, 430070 Wuhan, China. [4] Department of Physics, University at Buffalo, State University of New York, Buffalo, NY 14260, USA. [5] CAS Center for Excellence in Topological Quantum Computation, University of Chinese Academy of Sciences, 100190 Beijing, P. R. China. [6] Beijing Academy of Quantum Information Sciences, 100193 Beijing, P. R. China. [7] These authors contributed equally: Ranran Cai, Yunyan Yao. ✉email: weihan@pku.edu.cn

Fundamental symmetry breaking and relativistic spin–orbit coupling give rise to interesting phenomena in quantum materials[1,2]. For over 60 years, the interplay between ferromagnetism and superconductivity, has offered a wealth of intriguing phenomena in ferromagnet (FM)/superconductor (SC) heterostructures[3–6]. However, to overcome a strong suppression of spin-singlet superconductivity by the FM's exchange field the platforms supporting spin-triplet pairing are sought. They are desirable for dissipationless spin currents in superconducting spintronics[5–7], and probing quantum materials[8], as well as for realizing elusive Majorana bound states to implement topological quantum computing[9,10]. The common expectation that spin-triplet pairing in superconducting spintronics requires complex FM multilayers, typically relying on noncollinear/spiral magnetization or half metals[3–6,11].

Here, we report the possible experimental evidence for the spin-triplet Andreev reflection and induced spin-triplet superconductivity at the interface of a quasi-2D van der Waals (vdW) FM and a conventional *s*-wave SC with Rashba spin–orbit coupling (SOC). Such vdW heterostructures offer a great versatility in exploring the interplay between ferromagnetism and superconductivity, beyond the lattice-matching constraints of all-epitaxial FM/SC heterostructures[12]. Our results pave the way for future studies on spin-triplet superconductivity[13,14] and the formation on Majorana bound states[9,10], as well as many normal-state spintronic applications[15].

Results and discussion

Spin-triplet Andreev reflection and spin-triplet MR. In contrast to the conventional Andreev reflection at the FM/SC interface (Fig. 1a), an incident spin-up electron forms a spin-singlet Cooper pair in the ordinary SC with a reflected spin-down hole in the FM, spin-triplet Andreev reflection generates the spin-up hole with an injection of an equal-spin triplet Cooper pair in the spin-triplet SC (Fig. 1b). Due to Rashba SOC[16,17], spin-rotation symmetry is broken for the superconducting pairing (Fig. 1c), which acts as a spin-mixing described in conventional FM/SC heterostructures[5,6]. The broken spin-rotation symmetry leads to the spin-singlet paring ($m = 0, S = 0$) (S is the total spin quantum

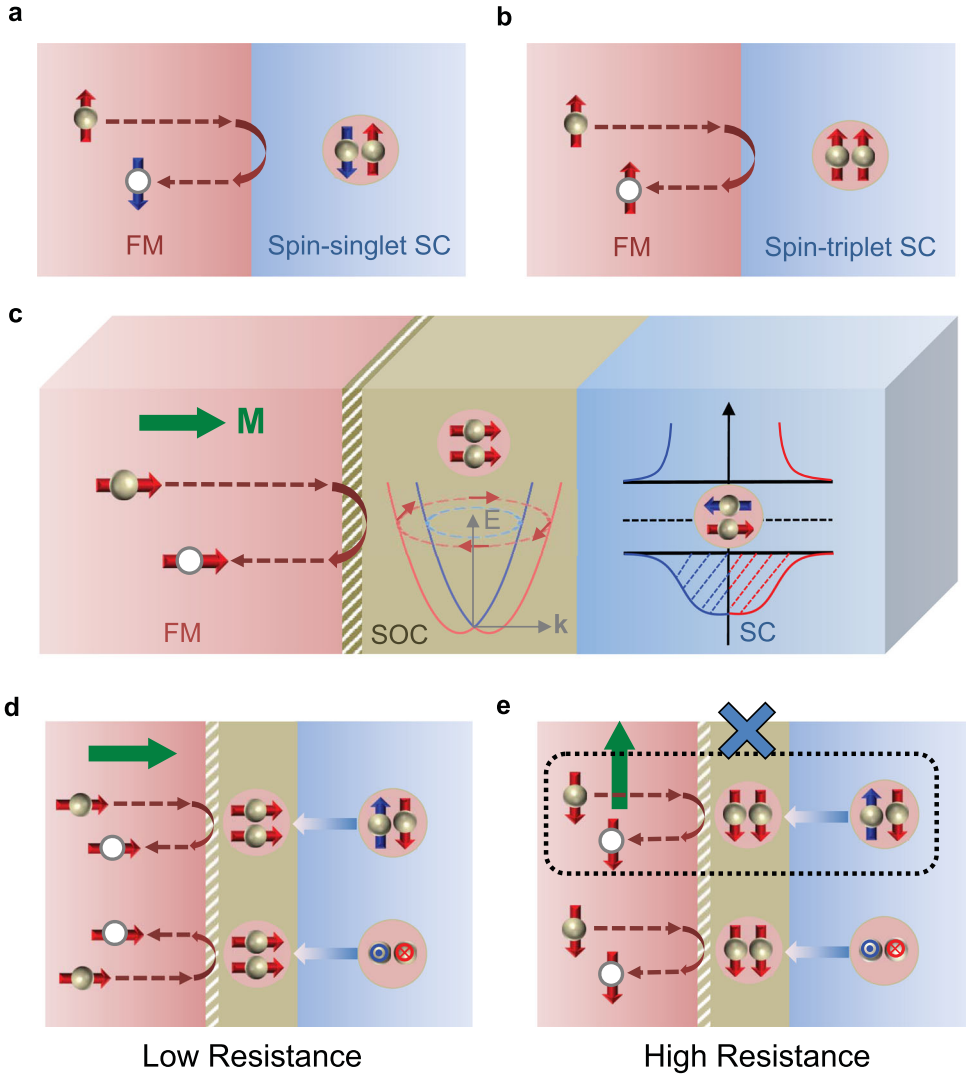

Fig. 1 Schematic of the spin-triplet Andreev reflection at FM/SC interface. a Conventional Andreev reflection at the FM/spin-singlet SC interface. **b** The spin-triplet Andreev reflection at the FM/spin-triplet SC interface. **c** Schematic of the spin-triplet Andreev reflection resulting from Rashba SOC at the interface between a FM and a conventional *s*-wave SC. The arrows in Rashba SOC band indicate spin-momentum locking and the red arrows represent the spin-polarization direction of equal-spin-triplet pairs. **d**, **e** Anisotropic spin-triplet Andreev reflection at the FM/SC interface and the low/high interfacial resistance states that depend on the FM magnetization direction, **M** (green arrow). Red arrows at the interface denote the spin direction of equal-spin-triplet pairs. For **M** along the interface the spin-triplet Andreev reflection can be suppressed.

number, and m is magnetic quantum number) with an unpolarized spin-triplet component ($m = 0$, $S = 1$)[18]. The spin-triplet component results in the interface spin-triplet Andreev reflection at the FM/SC interface which is highly anisotropic (Supplementary Note 1 and Supplementary Fig. 1), depending on the relative orientation between the magnetization (**M**) in the FM and the interfacial spin–orbit field[14,19]. **M** sets the spin-quantization axis, and unpolarized spin-triplet component ($m = 0$, $S = 1$) is projected onto the spin-quantization axis to generate the equal-spin-triplet component ($m = 1$, $S = 1$), which can be considered as a spin-rotation process[5]. For example, for FM magnetization along z axis (perpendicular to the interface), unpolarized spin-triplet Cooper pairs component $\left(|S = 1, S_y = 0\rangle \text{ and } |S = 1, S_x = 0\rangle\right.$ can be projected to the spin quantization axis as $|S = 1, S_z = 1\rangle$ due to the spin rotation process (S_y, S_x, and S_z are the spin quantum numbers along y, x, and z direction, respectively). Thus, both the $|S = 1, S_y = 0\rangle$ and $|S = 1, S_x = 0\rangle$ components will contribute to the interface conductance when **M** is perpendicular to interface, as illustrated in Fig. 1d. On the other hand, when the **M** is parallel to the interface along y direction, the equal-spin triplet Cooper pairs ($|S = 1, S_y = 1\rangle$) can only be projected from unpolarized spin-triplet pairing component $|S = 1, S_x = 0\rangle$, since $\left[S_x, S_y\right] \neq 0$. Consequently, spin-triplet Andreev reflection conductance channel is suppressed when **M** is parallel to interface, as illustrated in Fig. 1e. As a result of the anisotropic spin-triplet Andreev reflection processes, there is a low-resistance (high-resistance) state for **M** out-of-plane (in-plane) (Fig. 1d, e). Hence, the spin-triplet Andreev reflection can lead to the tunneling anisotropic magnetoresistance (MR) at the FM/SC interface, a proposed hallmark of the interfacial SOC and spin-triplet superconductivity in FM/SC heterostructures[14,19].

To experimentally probe the anisotropic spin-triplet Andreev reflection and spin-triplet MR, we fabricate the FM/SC devices (see "Methods" section for details), which consist of a quasi-2D vdW $Fe_{0.29}TaS_2$ flake, several s-wave superconducting NbN electrodes, and two normal metal Pt electrodes (Fig. 2a and Supplementary Fig. 2). At the interface between the quasi-2D vdW $Fe_{0.29}TaS_2$ flake and s-wave NbN electrode, the Cooper pairing consists of both spin-singlet ($m = 0$, $S = 0$) and spin-triplet components ($m = 0$, $S = 1$) due to the spin-rotation symmetry breaking by the interfacial Rashba SOC (right panel of Fig. 2a). The superconducting critical temperature of the NbN electrode is $T_{SC} \sim 12.5$ K (Supplementary Fig. 3a) characterized by standard four-probe electrical measurement. $Fe_{0.29}TaS_2$ flakes are typical quasi-2D vdW FM, with a Curie temperature, T_{Curie}, ~ 90 K, characterized by anomalous Hall effect (Supplementary Fig. 4)[20]. The magnetic easy axis is perpendicular to the sample plane, and **M** of $Fe_{0.29}TaS_2$ can be controlled by a large external magnetic field (**B**) (Supplementary Note 2 and Supplementary Fig. 5). For an in-plane $\mathbf{B} = 9$ T, **M** is almost in plane, 83° from the z direction. Under $\mathbf{B} = 9$ T, the current–voltage characteristics of the NbN electrode are measured, with critical currents of ~ 50 μA at $T = 2$ K (Supplementary Fig. 4b). Typical dI/dV curves of the $Fe_{0.29}TaS_2$/SC junctions as a function of T and **B** are shown in Supplementary Note 3 and Supplementary Fig. 6.

To characterize the expected MR arising from anisotropic spin-triplet Andreev reflection, the interfacial resistance between the quasi-2D vdW FM $Fe_{0.29}TaS_2$ and SC electrode is measured using the three-terminal geometry (Fig. 2a and see "Methods" section). Figure 2b shows the typical MR curve (blue) measured (device A; Supplementary Fig. 2) as a function of the magnetic field angle in the yz plane (Θ_{yz}) at $T = 2$ K and $\mathbf{B} = 9$ T. The observed MR shows a strong correlation with **B**-controlled **M** (Supplementary Fig. 7). In contrast to this large MR at $T = 2$ K, the normal-state interfacial resistance exhibits little variation at $T = 20$ K. A possible important contribution of vortices in type-II SC to the observed MR has been ruled out from our control measurements on normal metal/SC heterostructures at $T = 2$ K (orange curve in Fig. 2b and Supplementary Note 4 and Supplementary Fig. 8). We have also fabricated the control devices of $Fe_{0.29}TaS_2/Al_2O_3$/normal metal (Al), where no MR could be observed at $T = 2$ K (Supplementary Fig. 9), which further indicates the critical role of SC for the observed MR. Furthermore, the π-periodic oscillation further supports that the observed MR results from the anisotropic feature of spin-triplet Andreev reflection at the interface with Rashba SOC[14]. Figure 2c shows the MR results measured on the device B as a function of Θ_{yz} at $T = 2$ K and $\mathbf{B} = 9$ T. The MR ratio can be defined as:

$$\mathrm{MR}(\Theta_{yz}) = \frac{R(\Theta_{yz}) - R(\Theta_{yz} = 0)}{R(\Theta_{yz} = 0)} \times 100\%. \quad (1)$$

The $R(\Theta_{yz} = 0)$ and $R(\Theta_{yz} = 90)$ are the interfacial resistances for magnetic field that is perpendicular and parallel (along z and y directions in Fig. 2a) to the FM/SC interface, respectively. Interestingly, the observed MR ratio is ~ 37 ± 2% for device A, and ~ 103 ± 4% for device B, which are much larger than previous reports on the tunneling anisotropic MR in FM/semiconductor heterostructures arising from the Rashba and Dresselhaus SOC[16,17].

Temperature evolution of spin-triplet MR. Next, we investigate the temperature evolution of the MR to distinguish the contributions from the spin-triplet Andreev reflection and spin-dependent scattering by Bogoliubov quasiparticles under large magnetic field. Figure 3a shows the MR (Θ_{yz}) for device B at $T =$ 2, 4, 8, and 9 K, respectively, under the magnetic field of $\mathbf{B} = 5$ T. Figure 3b summarizes temperature dependence of the MR ratio for device B measured at $\mathbf{B} = 9$, 7, and 5 T, respectively. The MR appears for $T < T_C$, and starts to saturate below the temperature of ~5 K. The MR is no longer observable for $T \sim T_C$ at $\mathbf{B} = 9$, 7, and 5 T (Supplementary Fig. 10). Clearly, there is no enhancement or any anomaly of the MR observed at the temperature slightly below T_C, which further confirms that contribution from spin-dependent scattering by Bogoliubov quasiparticles is negligible[21,22].

Voltage dependence of spin-triplet MR. To further investigate the MR at the quasi-2D vdW FM $Fe_{0.29}TaS_2$/SC interface, we systematically vary the bias voltage (V_{bias}), which also affect the junction voltage (V_{3T}) across the interface. At the interface, the induced SC energy gap (Δ_{In}) by SC proximity effect with spin-triplet component is smaller compared to the SC gap (Δ_{NbN}) of bulk NbN electrode, as illustrated in Fig. 4a. When the potential (eV_{3T}) of the incoming electrons is considerably smaller than the interface spin-triplet superconducting energy gap (Δ_{In}) (Fig. 4a), the charge transport channel is dominated by the anisotropic spin-triplet Andreev reflection. Hence, the spin-triplet MR exhibits little variation with the eV_{3T} within the Δ_{In}. As the V_{3T} increases, other isotropic transport processes, such as electron-like and hole-like tunneling transmissions[14], also contribute to the interface conductance. As these transport processes are **M**-independent, the spin-triplet MR ratio is expected to decrease significantly. Since the change of V_{3T} is much smaller than V_{bias} during the rotation of the external magnetic field, the junction voltage for $\Theta_{yz} = 0$ (V_{3T_0}) is used to qualitatively show the interface voltage dependence of the spin-triplet MR. Figure 4b, c summarize these results measured on devices B and C. For small V_{3T_0}, the MR exhibit little variation as the voltage changes. However, when V_{3T_0} is higher than a critical value, MR strongly decreases as V_{3T}

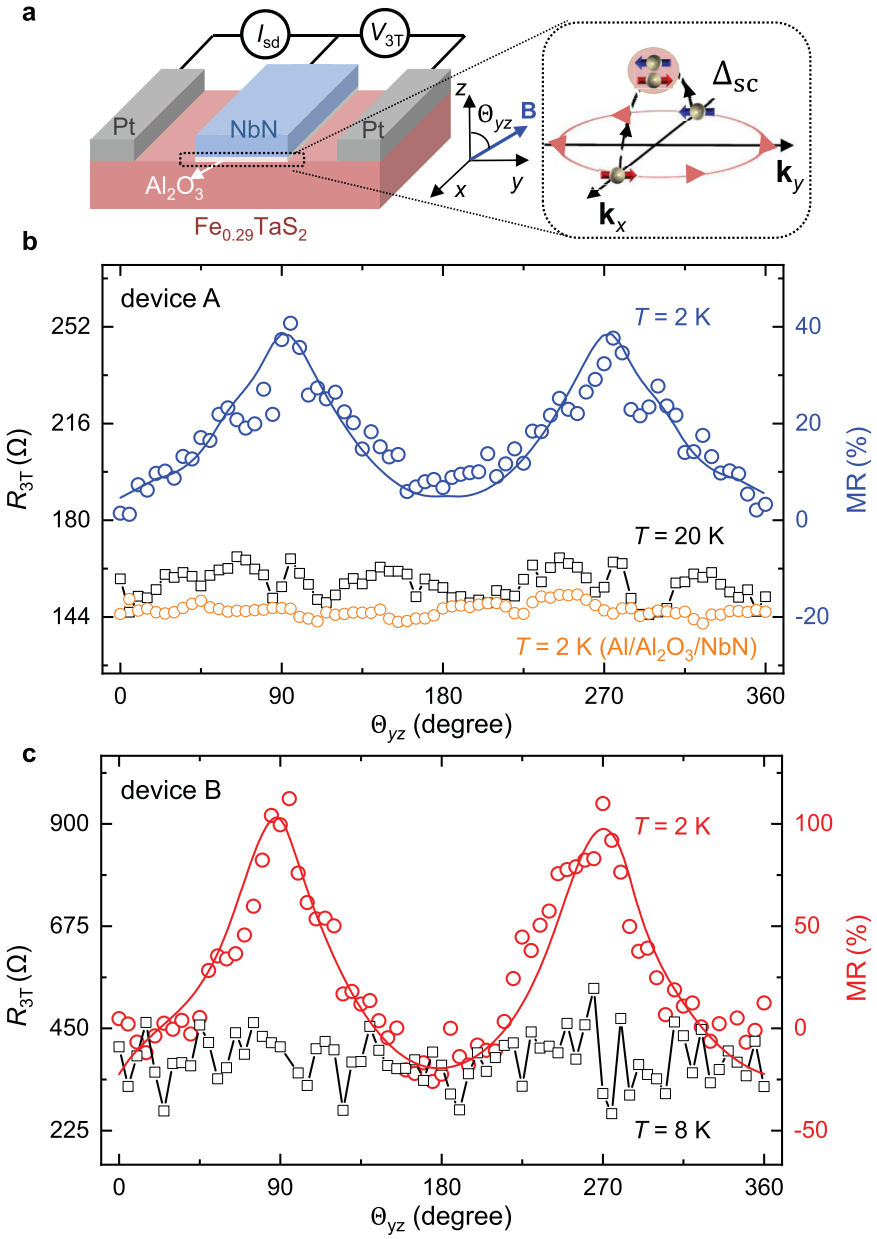

Fig. 2 Large magnetoresistance of the quasi-2D vdW $Fe_{0.29}TaS_2$/SC junction. a Illustration of the quasi-2D vdW $Fe_{0.29}TaS_2$/SC MR device and the measurement geometry. The right panel shows the schematic of the spin-triplet pairing component resulting from Rashba SOC at the FM/SC interface. **b** The interfacial resistance ($R_{3T} = V_{3T}/I_{sd}$) and MR ratio as a function of the magnetic field angle measured on the typical quasi-2D vdW $Fe_{0.29}TaS_2$/SC device (device A) under $\mathbf{B} = 9$ T. The orange curve represents the resistance measured on a typical control device (Al/Al_2O_3/NbN) under $\mathbf{B} = 9$ T. **c** The interfacial resistance and MR ratio as a function of the magnetic field angle on device B under $\mathbf{B} = 9$ T. The solid lines in **b** and **c** are guides to the eye.

increases. The critical junction voltage is obtained to be ~0.15 mV (~0.2 mV) for device B (C). We note that at 2 K the thermal energy is k_BT ~ 0.17 meV, comparable to the critical electron potential from the bias-dependent results. Therefore, an accurate value of the proximity-induced superconducting gap is not able to be clearly resolved here, which will need future studies. Additionally, the bias dependence of the spin-triplet MR further confirms that the observed MR is correlated to the sub-gap properties, and is completely different form **B**-induced spin-splitting density of states at the gap edges of SC electrodes[23].

Interface barrier dependence of spin-triplet MR. As the spin-triplet Andreev reflection depends strongly on the FM and SC wave-function overlap, it is expected that the dimensionless interface barrier strength (Z) plays an important role in the spin-triplet MR[24,25]. To explore the influence of interface barrier strength on the observed spin-triplet MR, we investigate more than dozen devices that are fabricated with Al_2O_3 layer of different thickness (~1–2.5 nm) between the quasi-2D vdW FM $Fe_{0.29}TaS_2$ and NbN SC electrodes. This process leads to a large range of interface resistance area product (R_JS) from ~10 to ~2000 Ω μm^2, resulting in the FM/SC heterostructures with very different Z-values. Figure 5 shows the measured MR ratio as a function of the R_JS at $T = 2$ K and $\mathbf{B} = 9$ T (Note: the MR is not observable for very large R_JS and not plotted in this figure). The largest MR is observed with R_JS ~ 48.4 Ω μm^2. The strong correlation of the MR ratio and R_JS reveals the important role of the Z-value in the spin-triplet MR.

This surprising nonmonotonic MR dependence on R_JS agrees well with the theoretical expectations[14,25]. The effective barrier

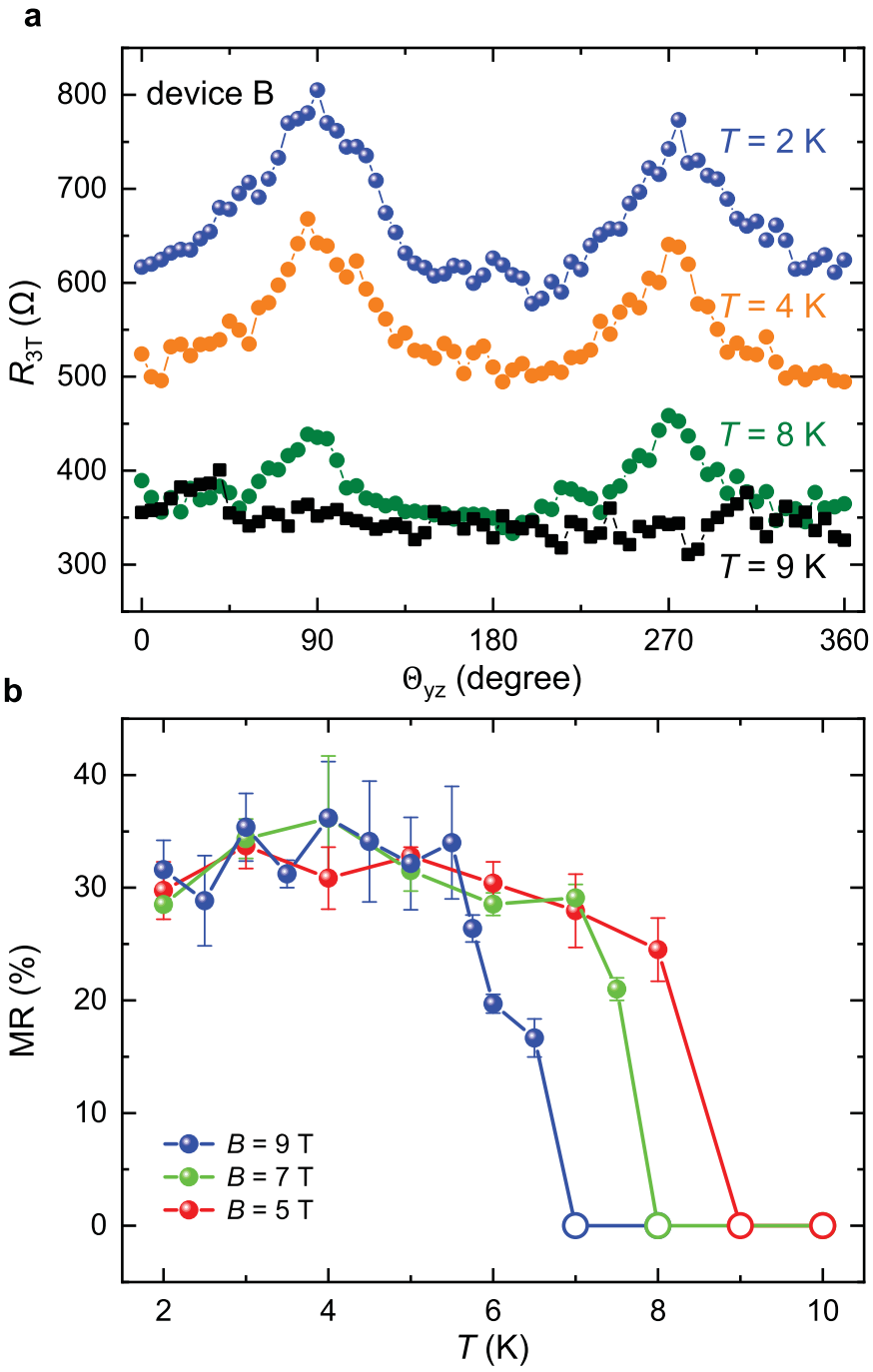

Fig. 3 The temperature dependence of MR at $Fe_{0.29}TaS_2$/SC interface. a The interfacial resistance as a function of Θ_{yz} measured on device B at $T = 2$ K (blue), 4 K (yellow) 8 K (olive), and 9 K (black), respectively. These results were obtained under $\mathbf{B} = 5$ T and $V_{bias} = 1$ mV, which correspond to V_{3T} ~ 0.40 mV for $T = 2$ and 4 K, and V_{3T} ~ 0.25 mV for $T = 8$ and 9 K. **b** The temperature dependence of MR ratio of device B at $\mathbf{B} = 9$ T, 7 T, and 5 T, respectively. The error bars correspond to one standard deviation. The open circles represent the absence of obvious MR.

strength is modified by SOC and depends on the helicity (outer/inner Rashba bands, Fig. 1b), $Z_{\pm} = Z \pm \bar{\gamma}k_{\parallel}$, where $\bar{\gamma}$ is the SOC parameter[25] and $k_{\parallel}$ is the component of the wave vector along the interface (Fig. 5 inset). At zero $k_{\parallel}$, the vanishing of Rashba SOC does not support spin-triplet component. At nonzero $k_{\parallel}$, increasing Z can reduce $|Z_+|$ or $|Z_-|$ and thus enhance such a transmission for a given helicity. For much larger Z, all of the conduction channels, including spin-triplet Andreev reflection, are suppressed due to the low interface transparency. As a result, the spin-triplet Andreev reflection and spin-triplet MR will also be nonmonotonic in Z. Taken together, the observed nonmonotonic MR dependence with R_IS (Fig. 5) and MR decrease with T or an applied voltage (Figs. 2–4) are all experimental evidence for the spin-triplet Andreev reflection in our vdW heterostructures. We note that the spin-triplet MR theory is developed using an idealized model of ballistic systems[14,25], the role of disorder, which could induce reflectionless tunneling, is expected to reduce the MR amplitude. To the best of our understanding, the spin-triplet Andreev reflection is the major cause for the observation of large MR up to ~103 ± 4%, and can qualitatively explain the bias

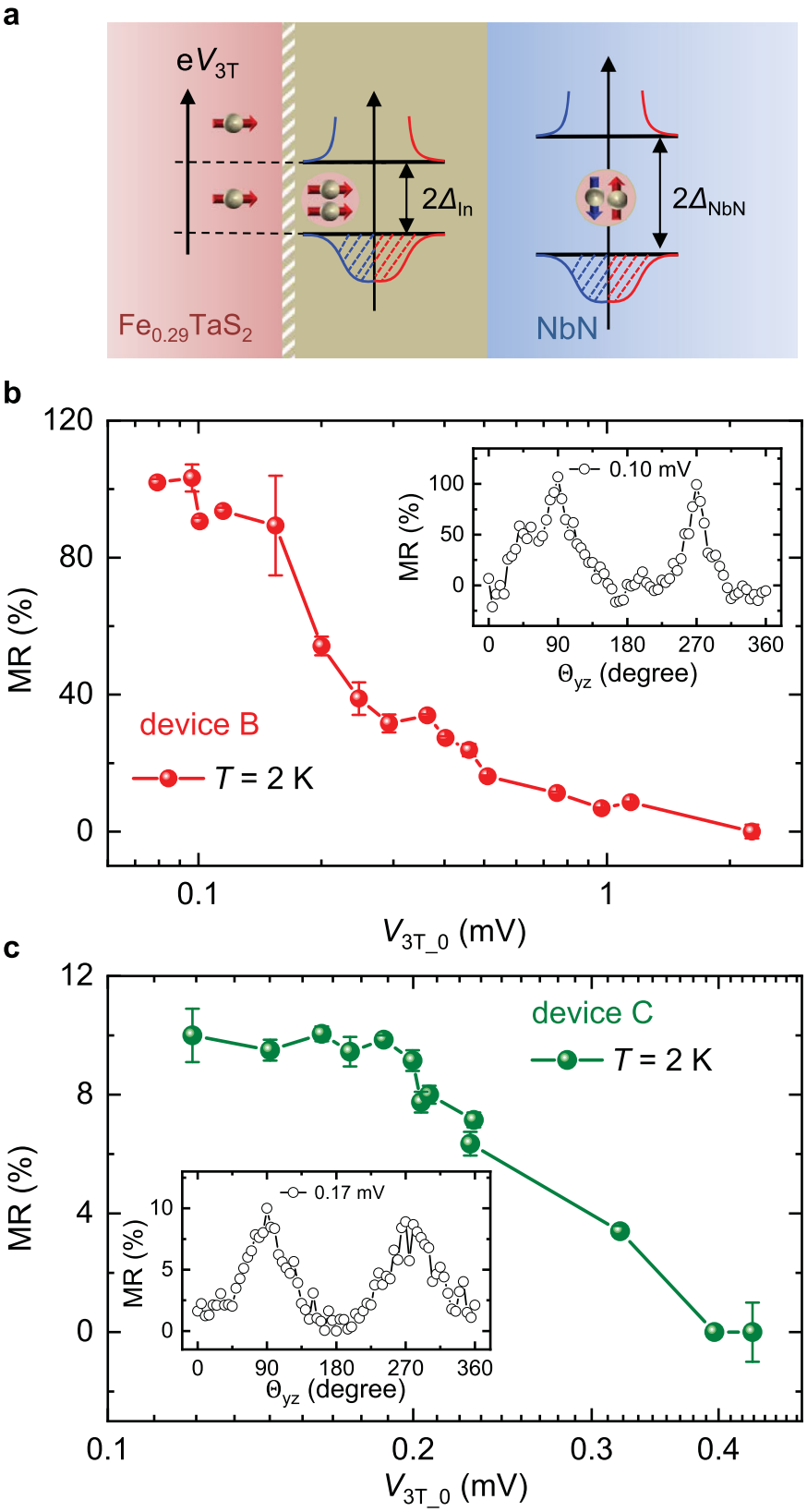

Fig. 4 The voltage dependence of MR at $Fe_{0.29}TaS_2$/SC interface. a Schematic of the incident spin-polarized electrons with chemical potentials inside and above the interface spin-triplet superconducting energy gap. Δ_{In} and Δ_{NbN} indicate the superconducting energy gaps of the interface SC and the bulk NbN. **b** The voltage dependence (V_{3T_0}) of the MR ratio of device B measured at $T = 2$ K and $\mathbf{B} = 9$ T. V_{3T_0} represents V_{3T} when an applied magnetic field is perpendicular to the FM/SC interface. The error bars correspond to one standard deviation. Inset: The typical MR curve at $V_{3T\_0} = 0.10$ mV. **c** The voltage dependence (V_{3T_0}) of the MR ratio of device C measured at $T = 2$ K and $\mathbf{B} = 9$ T. The error bars correspond to one standard deviation. Inset: The typical MR curve at $V_{3T\_0} = 0.17$ mV.

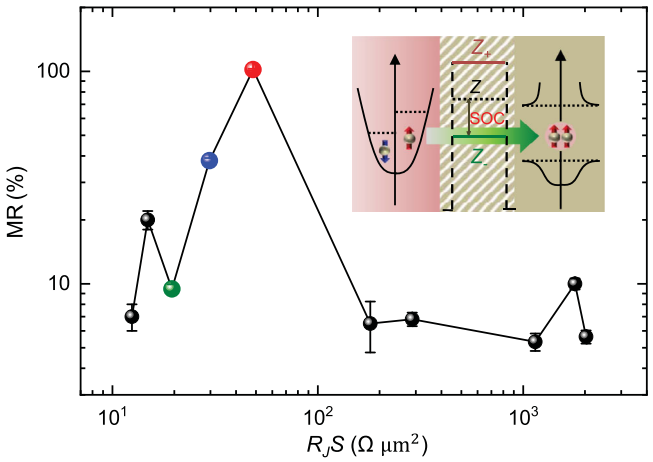

Fig. 5 The interface barrier dependence of MR at $Fe_{0.29}TaS_2$/SC interface. The MR ratio as a function of the interface resistance area product (R_JS) measured on various devices in the low voltage bias region. Inset: Schematic of the incident spin-polarized electrons into the interfacial spin-triplet SC via interface barrier with Rashba SOC. The Rashba SOC modifies the interface barrier strength (Z) to be $Z_\pm = Z \pm \bar{\gamma}k_\parallel$, where $\bar{\gamma}$ is the SOC parameter and $k_\parallel$ is the in-plane wave vector[25]. The blue, red, and green dots represent the MR of devices A, B, and C, respectively. The error bars correspond to one standard deviation.

and temperature dependence of the MR. Given the growing interest in systems that could support spin-triplet superconductivity, in the future studies, it would be important to generalize our description and also include the effects of disorder and diffusive transport on spin-triplet MR.

Summary and outlook. Our experimental obervation of a large tunneling anisotropic MR in quasi-2D vdW FM/s-wave SC heterostructures up to ~103 ± 4% is already promising for spintronic applications and much larger than for the normal-state transport in previously measured heterostructures with a single FM layer[16,17]. More importantly, this result also reveals an emergent spin-triplet superconductivity which, through spin-triplet Andreev reflection, is a sensitive probe of interfacial Rashba SOC. With the advances towards high-quality vdW heterostructures, we anticipate that the magnitude of such spin-triplet MR can be further enhanced and strongly modulated using different 2D vdW FMs due to their highly-tunable Rashba SOC by electric fields[26–29]. This tantalizing opportunity to implement FM/SC heterostructures to design and probe interfacial SOC offers an important boost for superconducting spintronics[3–6,30,31] and Majorana bounds states[9,32]. Furthermore, our quasi-2D platform of proximity-induced spin-triplet superconductivity, combined with the gate-controlled 2D vdW ferromagnetism[28,29,33] could provide tunable magnetic textures to create synthetic SOC[34] and braid Majorana bound states[35].

Methods

Device fabrication. The quasi-2D vdW $Fe_{0.29}TaS_2$/SC spin-triplet MR devices were fabricated as follows. First, bulk single crystalline $Fe_{0.29}TaS_2$ were grown by the iodine vapor transport method. Then the quasi-2D vdW $Fe_{0.29}TaS_2$ flakes were mechanical exfoliated from the bulk single crystal onto the SiO_2 (~300 nm)/Si substrates[20]. Second, a first-step electron-beam lithography was used to define the SC electrodes on the quasi-2D vdW $Fe_{0.29}TaS_2$ flakes. The SC electrodes consist of ~5 nm thick Nb and ~60 nm thick NbN, which were grown in a DC magneton sputtering system with a base pressure of ~1.2×10^{-4} Pa. Prior to the growth of SC electrodes, a thin Al_2O_3 layer (~1–2.5 nm) is deposited as the barrier to tune the interface coupling strength between the quasi-2D vdW $Fe_{0.29}TaS_2$ flakes and the SC electrodes. The Al_2O_3 layer was grown by DC magnetron sputtering with Al target under the oxygen atmosphere. Then, a second-step electron-beam lithography was used to define the two normal Pt electrodes (~80 nm) on the quasi-2D vdW $Fe_{0.29}TaS_2$ flakes. The Pt electrodes were deposited by RF magneton sputtering in a system with a base pressure lower than 6.5×10^{-4} Pa. The optical images of three typical devices (A, B, and C) are shown in Fig. S2.

Spin-triplet MR measurement. The MR measurement of the quasi-2D vdW $Fe_{0.29}TaS_2$/SC devices was performed in a Physical Properties Measurement System (PPMS; Quantum Design). A bias (V_{bias}) was applied between the SC electrode and one normal Pt electrode using a Keithley K2400, the source–drain current (I_{sd}) was measured using the same K2400, and the voltage (V_{3T}) between the SC electrode and the other Pt electrode was measured using a Keithley 2002. The interfacial resistance was obtained via dividing the three-terminal voltage by the source–drain current ($R_{3T} = V_{3T}/I_{sd}$). During the measurement of each spin-triplet MR curve, the quasi-2D vdW $Fe_{0.29}TaS_2$/SC device was rotated from 0 to 360 degrees under the external static magnetic field in the PPMS.

Data availability

The data that support the findings of this study are available from the corresponding authors upon request.

Received: 21 June 2021; Accepted: 1 November 2021;
Published online: 18 November 2021

References

1. Tokura, Y., Kawasaki, M. & Nagaosa, N. Emergent functions of quantum materials. *Nat. Phys.* **13**, 1056–1068 (2017).
2. Basov, D. N., Averitt, R. D. & Hsieh, D. Towards properties on demand in quantum materials. *Nat. Mater.* **16**, 1077–1088 (2017).
3. Bergeret, F. S., Volkov, A. F. & Efetov, K. B. Odd triplet superconductivity and related phenomena in superconductor-ferromagnet structures. *Rev. Mod. Phys.* **77**, 1321–1373 (2005).
4. Buzdin, A. I. Proximity effects in superconductor-ferromagnet heterostructures. *Rev. Mod. Phys.* **77**, 935–976 (2005).
5. Linder, J. & Robinson, J. W. A. Superconducting spintronics. *Nat. Phys.* **11**, 307–315 (2015).
6. Eschrig, M. Spin-polarized supercurrents for spintronics: a review of current progress. *Rep. Prog. Phys.* **78**, 104501 (2015).
7. Jeon, K.-R. et al. Enhanced spin pumping into superconductors provides evidence for superconducting pure spin currents. *Nat. Mater.* **17**, 499–503 (2018).
8. Han, W., Maekawa, S. & Xie, X.-C. Spin current as a probe of quantum materials. *Nat. Mater.* **19**, 139–152 (2020).
9. Sau, J. D., Lutchyn, R. M., Tewari, S. & Das Sarma, S. Generic new platform for topological quantum computation using semiconductor heterostructures. *Phys. Rev. Lett.* **104**, 040502 (2010).
10. Aasen, D. et al. Milestones toward Majorana-based quantum computing, *Phys. Rev. X* **6**, 031016 (2016).
11. Visani, C. et al. Equal-spin Andreev reflection and long-range coherent transport in high-temperature superconductor/half-metallic ferromagnet junctions. *Nat. Phys.* **8**, 539–543 (2012).
12. Martínez, I. et al. Interfacial spin–orbit coupling: a platform for superconducting spintronics. *Phys. Rev. Appl.* **13**, 014030 (2020).
13. Bergeret, F. S. & Tokatly, I. V. Spin–orbit coupling as a source of long-range triplet proximity effect in superconductor-ferromagnet hybrid structures. *Phys. Rev. B* **89**, 134517 (2014).
14. Högl, P., Matos-Abiague, A., Žutić, I. & Fabian, J. Magnetoanisotropic Andreev reflection in ferromagnet-superconductor junctions. *Phys. Rev. Lett.* **115**, 116601 (2015).
15. Žutić, I., Fabian, J. & Das Sarma, S. Spintronics: fundamentals and applications. *Rev. Mod. Phys.* **76**, 323–410 (2004).
16. Gould, C. et al. Tunneling anisotropic magnetoresistance: a spin-valve-like tunnel magnetoresistance using a single magnetic layer. *Phys. Rev. Lett.* **93**, 117203 (2004).
17. Moser, J. et al. Tunneling anisotropic magnetoresistance and spin–orbit coupling in Fe/GaAs/Au tunnel junctions. *Phys. Rev. Lett.* **99**, 056601 (2007).
18. Gor'kov, L. P. & Rashba, E. I. Superconducting 2D system with lifted spin degeneracy: mixed singlet-triplet state. *Phys. Rev. Lett.* **87**, 037004 (2001).
19. Lv, P., Zhou, Y.-F., Yang, N.-X. & Sun, Q.-F. Magnetoanisotropic spin-triplet Andreev reflection in ferromagnet-Ising superconductor junctions. *Phys. Rev. B* **97**, 144501 (2018).
20. Cai, R. et al. Anomalous Hall effect mechanisms in the quasi-two-dimensional van der Waals ferromagnet $Fe_{0.29}TaS_2$. *Phys. Rev. B* **100**, 054430 (2019).
21. Tinkham, M. *Introduction to Superconductivity*. (Dover Publications, 2004).

22. Yao, Y. et al. Probe of spin dynamics in superconducting NbN thin films via spin pumping. *Phys. Rev. B* **97**, 224414 (2018).
23. Meservey, R. & Tedrow, P. M. Spin-polarized electron tunneling. *Phys. Rep.* **238**, 173 (1994).
24. Blonder, G. E., Tinkham, M. & Klapwijk, T. M. Transition from metallic to tunneling regimes in superconducting microconstrictions: excess current, charge imbalance, and supercurrent conversion. *Phys. Rev. B* **25**, 4515–4532 (1982).
25. Vezin, T., Shen, C., Han, J. E. & Žutić, I. Enhanced spin-triplet pairing in magnetic junctions with s-wave superconductors. *Phys. Rev. B* **101**, 014515 (2020).
26. Gong, C. & Zhang, X. Two-dimensional magnetic crystals and emergent heterostructure devices. *Science* **363**, eaav4450 (2019).
27. Burch, K. S., Mandrus, D. & Park, J.-G. Magnetism in two-dimensional van der Waals materials. *Nature* **563**, 47–52 (2018).
28. Mak, K. F., Shan, J. & Ralph, D. C. Probing and controlling magnetic states in 2D layered magnetic materials. *Nat. Rev. Phys.* **1**, 646–661 (2019).
29. Gibertini, M., Koperski, M., Morpurgo, A. F. & Novoselov, K. S. Magnetic 2D materials and heterostructures. *Nat. Nanotechnol.* **14**, 408–419 (2019).
30. T. S. Khaire et al., Observation of Spin-Triplet Superconductivity in Co-Based Josephson Junctions. *Phys. Rev. Lett.* **104**, 137002 (2010).
31. Banerjee, N., Robinson, J. W. A. & Blamire M. G. Reversible contol of spin-polarized supercurrents in ferromagnetic Josephson junctions. *Nat. Commun.* **5**, 4771 (2014).
32. Zhang, H., Liu, D. E., Wimmer, M. & Kouwenhoven, L. P. Next steps of quantum transport in Majorana nanowire devices. *Nat. Commun.* **10**, 5128 (2019).
33. Deng, Y. et al. Gate-tunable room-temperature ferromagnetism in two-dimensional Fe_3GeTe_2. *Nature* **563**, 94–99 (2018).
34. Desjardins, M. M. et al. Synthetic spin–orbit interaction for Majorana devices. *Nat. Mater.* **18**, 1060–1064 (2019).
35. Fatin, G. L., Matos-Abiague, A., Scharf, B. & Žutić, I. Wireless Majorana bound states: from magnetic tunability to braiding. *Phys. Rev. Lett.* **117**, 077002 (2016).

Acknowledgements

We thank E. I. Rashba for valuable discussions. R.C., Y.Y., Y.M., W.X., B.L., Y.J., H.Z., S.J., X.C.X., Q.-F.S., and W.H. acknowledge the financial support from National Basic Research Programs of China (Nos. 2019YFA0308401, 2017YFA0303301, and 2018YFA0305601), National Natural Science Foundation of China (Nos. 11974025, 11921005, 11947053, 11774007, and U1832214), Beijing Natural Science Foundation (No. 1192009), and the Key Research Program of the Chinese Academy of Sciences (Grant No. XDB28000000). P.L. also acknowledges the financial support from Hubei Provincial Natural Science Foundation of China (No. 2019CFB218). C.S. and I.Z. acknowledge the support from U.S. Department of Energy, Office of Science, Basic Energy Sciences under Award No. DE- SC0004890.

Author contributions

R.C., W.X., and B.L. prepared the 2D van der Waals ferromagnet $Fe_{0.29}TaS_2$ flakes and fabricated the devices. R.C., Y.Y., Y.M., and Y.J. performed the MR measurements. P.L., C.S., X.C.X., I.Z., and Q.-F.S. performed the theoretical analysis. H.Z. and S.J. synthesized the bulk $Fe_{0.29}TaS_2$ single crystals. W.H. supervised the experiments and wrote the manuscript with contributions from all authors. All the authors discussed the results and contributed to the final version of the manuscript.

Competing interests

The authors declare no competing interests.

Additional information

Supplementary information The online version contains supplementary material available at https://doi.org/10.1038/s41467-021-27041-w.

Correspondence and requests for materials should be addressed to Wei Han.

Peer review information *Nature Communications* thanks Javier Villegas, Zhe Wang and the other, anonymous, reviewer(s) for their contribution to the peer review of this work.

Reprints and permission information is available at http://www.nature.com/reprints

Publisher's note Springer Nature remains neutral with regard to jurisdictional claims in published maps and institutional affiliations.